Probabilistic Projections of Climate Change over China under the SRES A1B Scenario Using 28 AOGCMs

WEILIN CHEN AND ZHIHONG JIANG

Key Laboratory of Meteorological Disaster of Ministry of Education, Nanjing University of Information Science and Technology, Nanjing, China

LAURENT LI

Laboratoire de Météorologie Dynamique, IPSL/CNRS/UPMC, Paris, France

(Manuscript received 28 September 2010, in final form 27 January 2011)

ABSTRACT

Probabilistic projection of climate change consists of formulating the climate change information in a probabilistic manner at either global or regional scale. This can produce useful results for studies of the impact of climate change impact and change mitigation. In the present study, a simple yet effective approach is proposed with the purpose of producing probabilistic results of climate change over China for the middle and end of the twenty-first century under the Special Report on Emissions Scenarios A1B (SRES A1B) emission scenario. Data from 28 coupled atmosphere–ocean general circulation models (AOGCMs) are used. The methodology consists of ranking the 28 models, based on their ability to simulate climate over China in terms of two model evaluation metrics. Different weights were then given to the models according to their performances in present-day climate. Results of the evaluation for the current climate show that five models that have relatively higher resolutions—namely, the Istituto Nazionale di Geofisica e Vulcanologia ECHAM4 (INGV ECHAM4), the third climate configuration of the Met Office Unified Model (UKMO HadCM3), the CSIRO Mark version 3.5 (Mk3.5), the NCAR Community Climate System Model, version 3 (CCSM3), and the Model for Interdisciplinary Research on Climate 3.2, high-resolution version [MIROC3.2 (hires)]—perform better than others over China. Their corresponding weights (normalized to 1) are 0.289, 0.096, 0.058, 0.048, and 0.044, respectively. Under the A1B scenario, surface air temperature is projected to increase significantly for both the middle and end of the twenty-first century, with larger magnitude over the north and in winter. There are also significant increases in rainfall in the twenty-first century under the A1B scenario, especially for the period 2070–99. As far as the interannual variability is concerned, the most striking feature is that there are high probabilities for the future intensification of interannual variability of precipitation over most of China in both winter and summer. For instance, over the Yangtze–Huai River basin (28°–35°N, 105°–120°E), there is a 60% probability of increased interannual standard deviation of precipitation by 20% in summer, which is much higher than that of the mean precipitation. In general there are small differences between weighted and unweighted projections, but the uncertainties in the projected changes are reduced to some extent after weighting.

1. Introduction

Projection of future climate change at regional scale is important for the assessment of climate change impacts, as well as the elaboration of appropriate mitigation and adaptation measures. Coupled atmosphere–ocean general circulation models (AOGCMs), along with adequate regionalization methods (e.g., regional climate models, statistical downscaling), are the most appropriate tools for projecting climate under scenarios of greenhouse gas emission. Considerable uncertainties exist in different steps of future climate projection. Those related to the representation of physical mechanisms in global coupled models are believed to be large but can be assessed through the approach of multimodel ensemble (MME). This implies naturally a probabilistic projection, which is also quite suitable for impact or mitigation studies. In fact, policy makers responsible for complex socioeconomic

Corresponding author address: Dr. Zhihong Jiang, Key Laboratory of Meteorological Disaster of Ministry of Education, Nanjing University of Information Science and Technology, Nanjing 210044, China.
E-mail: zhjiang@nuist.edu.cn

DOI: 10.1175/2011JCLI4102.1

plans and managements can take into account future climate projections expressed in a probabilistic manner.

As a result of recent coordinated efforts of the scientific community, a number of AOGCMs have been run to simulate the evolution of a climate system from preindustrial times to the end of the twenty-first century using historical observed and future scenarios of anthropogenic and natural forcings, producing large datasets of projection of future climate (Cubasch et al. 2001; Meehl et al. 2007). For instance, the recent World Climate Research Programme (WCRP) Coupled Model Intercomparison Project phase 3 (CMIP3; Meehl et al. 2007) consists of 23 state-of-the-art AOGCMs from 16 institutions and 11 countries. Model output from CMIP phase 5 (CMIP5) will also be available in the near future (Taylor et al. 2008). Multimodel databases offer both scientific opportunities and challenges in combining these datasets (Knutti et al. 2010).

Two main approaches have been developed to combine multimodel ensemble output (Tebaldi and Sanso 2009). One simply considers each model as equal and produces simple ensemble averages (''one model, one vote''). The other, which has been paid more and more attention nowadays, stems from the belief that not all models are to be trusted equally, but some are better than others and should receive more weight in the combination of the results. In recent years, a number of techniques have been proposed to weight the model (e.g., downweight or eliminate some ''bad'' climate models based on metrics of skill, Schmittner et al. 2005; Whetton et al. 2007; Santer et al. 2009; Perkins and Pitman 2009; Knutti 2010), such as the reliability ensemble average (REA) approach (Giorgi and Mearns 2002, 2003; Moise and Hudson 2008), which has been updated by Xu et al. (2010), as well as Bayesian methods (Tebaldi et al. 2004, 2005; Greene et al. 2006; Furrer et al. 2007; Tebaldi and Knutti 2007; Smith et al. 2009; Tebaldi and Sanso 2009). The REA and Bayesian methods have also been proposed to perform probabilistic projections of climate change at global and regional scales (Collins 2007), in which a climate change projection/prediction essentially consists of producing probability density functions (PDFs) or cumulative distribution functions (CDFs) of the changes in climatic variables of interest. The spread of the PDF is a measure of the uncertainty in the projection (Watterson 2008; Xu et al. 2010).

For China, a number of recent climate change simulations and projections with different AOGCMs have been analyzed (Jiang et al. 2004, 2005, 2009; Zhou and Yu 2006; Sun and Ding 2008, 2009; Li et al. 2010; among others). For example, based on the simulation outputs of 17 AOGCMs for the Intergovernmental Panel on Climate Change (IPCC) Fourth Assessment Report (AR4), Jiang et al. (2009) analyzed the spatial and temporal characteristics of the 1°–3°C warming over China in the twenty-first century. Sun and Ding (2009) investigated the future potential changes in precipitation and monsoon circulation in the summer in East Asia under the Special Report on Emissions Scenarios (SRES) A1B emission scenario. However, these studies are all based on the simple MME method, and there is little information about probabilistic projection for future evolution of climate change over this region.

In the present study, we attempt to construct probabilistic projections of climate change over China under the SRES A1B scenario in the twenty-first century based on a simple yet effective method. We first prequalify 28 available AOGCMs based on their ability to simulate climate over China in terms of two metrics of model skills. Then different weights are given to the models based on their performances in simulating present-day climate. We address the issue of uncertainties to some extent by interpreting the climate projection problem in a probabilistic way.

The paper is organized as follows: Section 2 provides a brief description of the datasets, model evaluation metrics, and the weighting methodology. Section 3 describes the results from the model-quality assessment. The probabilistic projections of climate change over China are presented and interpreted in section 4. In section 5, the projected changes provided by the weighted ensemble mean and the unweighted one are compared. Finally, section 6 provides a general discussion and conclusions.

2. Data and methods

a. Data

This study uses 22 coupled AOGCMs from the CMIP3 in support of the IPCC AR4, as well as 6 AOGCMs from the Ensemble-Based Predictions of Climate Changes and Their Impacts (ENSEMBLES) project (van der Linden and Mitchell 2009), which is funded by the European Commission. One ensemble member for each model is used. The models participating in the ENSEMBLES project, shown in bold in Table 1, are generally improved or extended versions of models contributing to the IPCC AR4 [through improvement to core physical schemes, and the inclusion or improvement of the carbon cycle component (CC), aerosol chemical transport component (AT), and transient land use change component (LU)]. A more detailed documentation of the ENSEMBLES models is described by van der Linden and Mitchell (2009). As a result, a total of 28 models (Table 1) were used in this study, which should be so far the most comprehensive projection under the A1B scenario over China.

TABLE 1. Model Identification, originating group/country, and atmospheric resolution. Models participating in the ENSEMBLES project are shown in bold.

Model ID	Originating group/country	Atmosphere resolution (°)
BCCR BCM2.0	Bjerknes Centre for Climate Research (BCCR)/Norway	2.8 × ~2.8
CGCM3.1 (T47)	Canadian Centre for Climate Modelling and Analysis (CCCma)/Canada	3.75 × ~3.75
CGCM3.1 (T63)	CCCMA/Canada	2.8 × ~2.8
CNRM-CM3	Centre National de Recherches Météorologiques (CNRM)/France	2.8 × ~2.8
CSIRO Mk3.0	CSIRO Atmospheric Research/Australia	1.875 × ~1.875
CSIRO Mk3.5	CSIRO Atmospheric Research/Australia	1.875 × ~1.875
GFDL CM2.0	Geophysical Fluid Dynamics Laboratory (GFDL)/United States	2.5 × 2.0
GFDL CM2.1	GFDL/United States	2.5 × 2.0
GISS-EH	National Aeronautics and Space Administration (NASA) GISS/United States	5 × 4
FGOALS-g1.0	National Key Laboratory of Numerical Modeling for Atmospheric Sciences and Geophysical Fluid Dynamics (LASG), Institute of Atmospheric Physics (IAP)/China	2.8 × 2.8
INGV ECHAM4	INGV/Italy	1.125 × ~1.125
INMCM3.0	Institute for Numerical Mathematics (INM)/Russia	5.0 × 4.0
IPSL_CM4	L'Institut Pierre-Simon Laplace (IPSL)/France	3.75 × 2.5
MIROC3.2(hires)	Center for Climate System Research, National Institute for Environmental Studies, and Frontier Research Center for Global Change (FRCGC)/Japan	1.125 × 1.12
MIROC3.2(medres)	Center for Climate System Research, National Institute for Environmental Studies, and FRCGC/Japan	2.8 × ~2.8
MIUBECHOG	Meteorological Institute of the University of Bonn, Meteorological Research Institute of the Korea Meteorological Administration (KMA), and Model and Data group/Germany and Korea	3.75 × ~3.75
ECHAM5/MPI-OM	Max Planck Institute for Meteorology (MPI)/Germany	1.875 × ~1.875
MRI CGCM2.3.2	Meteorological Research Institute (MRI)/Japan	2.8 × ~2.8
NCAR CCSM3	NCAR/United States	1.4 × ~1.4
NCAR PCM1	NCAR/United States	2.8 × ~2.8
UKMO HadCM3	Hadley Centre for Climate Prediction and Research, Met Office (UKMO)/ United Kingdom	3.75 × 2.5
UKMO HadGEM1	Hadley Centre for Climate Prediction and Research, Met Office/United Kingdom	1.875 × 1.25
CNRM-CM3.3, LU	Centre National de Recherches Météorologiques (CNRM)/France	2.8 × ~2.8
HadCM3C, CC&AT	Hadley Centre for Climate Prediction and Research, Met Office/United Kingdom	3.75 × 2.5
HadGEM2-AO, AT&LU	Hadley Centre for Climate Prediction and Research, Met Office/United Kingdin	1.875 × 1.25
INGV C-ESM, CC	INGV/Italy	3.75 × ~3.75
IPSL CM4 V2, LU	IPSL/France	2.5 × 1.268
ECHAM5_C, CC&LU	Max Planck Institute for Meteorology/Germany	3.75 × ~3.75

Monthly precipitation (Pr) and surface air temperature (Tas) fields from the Twentieth-Century Climate in Coupled Model (20C3M) runs and the SRES A1B emissions scenario runs are used in the analysis. The CO_2 concentration associated with the A1B scenarios is expected to reach a maximum of 720 ppm by 2100, according to Nakicenovic and Swart (2000). The IPCC AR4 simulation results were obtained from the FTP server (ftp://ftp-esg.ucllnl.org/) that is maintained by the Earth System Grid II (ESG) research project sponsored by the U.S. Department of Energy Office of Science. The ENSEMBLES simulation datasets are obtained from the Climate and Environmental Data Retrieval and Archive (CERA) database, run by the Model and Data group at the Max Planck Institute for Meteorology (www.mad.zmaw.de/projects-at-md/ensembles/).

Model performance is assessed by the University of East Anglia's Climate Research Unit time series (CRU TS2.1) temperature and precipitation datasets (Mitchell and Jones 2005; New et al. 2002). The model and observed data are regridded to a common 1.0° × 1.0° grid, with only land points being used in the interpolation. In this study we focus on climatology of the last 40 yr of the twentieth-century simulations (1960–99).

b. Model evaluation metrics

Models that do a good job for basic variables, such as surface air temperature and precipitation, often have good performance in other variables (e.g., Gleckler et al. 2008). Hence, we use these two basic variables to evaluate model performance.

1) MSE

According to Pierce et al. (2009), the mean-squared error (MSE) is defined as

$$\mathrm{MSE}(m,o) = \frac{1}{\mathrm{N}} \sum_{k=1}^{N} (M_k - O_k)^2, \quad (1)$$

where M_k and O_k indicate the model pattern of interest and the corresponding observed pattern, respectively, and N indicates the number of spatial points.

We transform this performance measure to a (dimensionless) spatial skill metric (M1) by normalizing as follows:

$$\mathrm{M1} = 1 - \frac{\mathrm{MSE}(m,o)}{\mathrm{MSE}(\overline{o},o)}, \quad (2)$$

where the overbar indicates the spatial mean. This normalization step enables us to compare climate variables (temperature and precipitation) with different units. A model field identical to observation has a M1 value of 1, and the closer the M1 value is to 1, the greater skill in simulating the spatial climatologies.

2) INTERANNUAL VARIABILITY

The variability is measured by the interannual standard deviation (STD). Before calculating the STD, there is no special filtering applied (Scherrer 2010); that is, interannual variability also contains some decadal variability strictly speaking, although we think the contribution from decadal variability is small. As in the study by Gleckler et al. (2008) and Santer et al. (2009), we calculate a ''symmetric'' variability statistic (M2), which has the same numeric values for a model that simulates half and twice the observed variability as follows:

$$\mathrm{M2} = \left(\frac{\mathrm{STD}_m}{\mathrm{STD}_o} - \frac{\mathrm{STD}_o}{\mathrm{STD}_m} \right)^2, \quad (3)$$

where STD_m denotes the interannual standard deviation of simulated variables and STD_o is the STD of observed variables. We first calculated the M2 value at each grid point over China and then compute the China-averaged value. It should be noted that M2 is also dimensionless. Moreover, the M2 value is equal to 0 when STD_m is identical to STD_o, and the closer the M2 value is to 0, the greater skill in simulating the interannual variability.

c. Weighting methodology

Compared with previously published methods for weighting simulations of climate change (e.g., the REA methods), the largest difference of our method is the weighting functions. We first rank all 28 models according to their order of performance in terms of each individual metric, as defined in section 2b. For each model we then obtain S_i, which is a simple sum of its ranks for the two individual metrics. The inverse of the normalized S_i can then be considered as a model reliability factor (R_i).

Let the sum of a model's ranks be S_i and let the sum of all models' ranks be $\sum_{i=1}^{N} S_i$; the model reliability factors is defined as

$$R_i = \frac{\sum_{i=1}^{N} S_i}{S_i}. \quad (4)$$

Evidently R_i can be thought as the combined ''model quality'' metric, representing one model's skill in simulating historical climatology. The greater the R_i value, the better is the skill. Once the reliability factor (R_i) for each model is calculated, the likelihood of a model's outcome is defined by

$$W_i = \frac{R_i}{\sum_{i=1}^{N} R_i}. \quad (5)$$

In fact W_i is just the normalized value of R_i (so that the sum of the weights across all 28 AOGCMs is equal to 1).Then threshold probabilities can be derived by summing over all W_i, which exceeds a given threshold of climate change. For example, the probability of a temperature change exceeding a certain threshold ΔT_{th} is given by Giorgi and Mearns (2003) and Xu et al. 2010 and is defined as

$$P^{\Delta T > \Delta T_{\mathrm{th}}} = \sum_i W_i, \quad \Delta T_i > \Delta T_{\mathrm{th}}. \quad (6)$$

Moreover, the probability of the change of a variable that is lower than the threshold ΔT_{th} can be obtained by $1 - P$. It should be pointed out that here we have made a reasonable starting assumption that better agreement with past climate builds more confidence in the reliability of a model's future projections (Whetton et al. 2007).

As in Giorgi and Mearns (2003), the weighted average change is given as

$$\Delta T = \frac{\sum_i W_i \Delta T_i}{\sum_i W_i}, \quad (7)$$

where ΔT_i is the projected change of model i and W_i is its corresponding weight defined by Eq. (5).

The uncertainty in projection is measured by the root-mean-square difference (RMSD) of the projected change (Giorgi and Mearns 2003; Xu et al. 2010). Here the term *difference* refers to the difference between one single

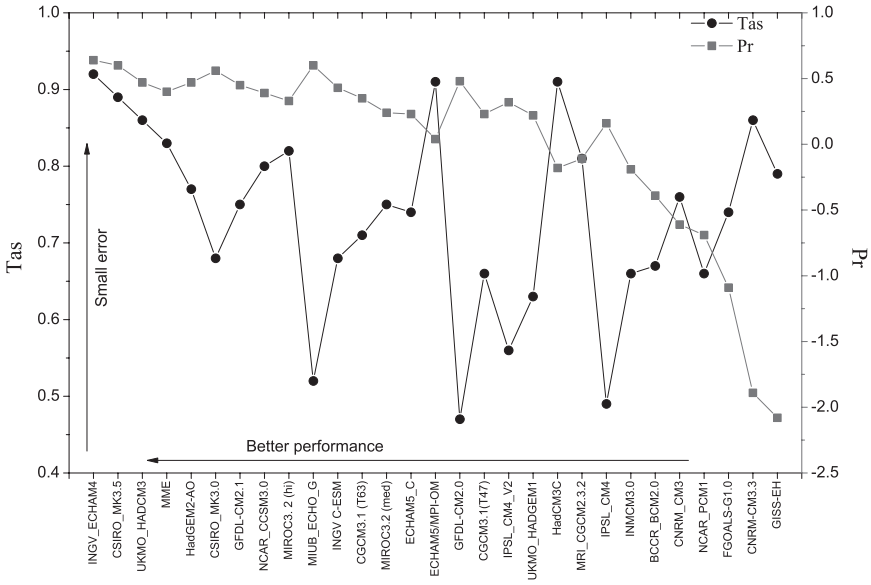

FIG. 1. Model skill scores (M1) of the spatial mean squared error of the temperature (left scale) and precipitation (right scale). The 28 AOGCMs and MMEs are ordered by the mean M1 value of the temperature and precipitation. Large values of M1 indicate good skill in simulating the spatial climatologies.

model's projected change and MME's projected one. For example, the RMSD of change projected by weighted averages and unweighted ones are defined by Eqs. (8) and (9) as follows:

$$\overline{\delta}_{\Delta T} = \left[\frac{\sum_i W_i (\Delta T_i - \Delta T)^2}{\sum_i W_i} \right]^{1/2} \quad \text{and} \tag{8}$$

$$\delta_{\Delta T} = \left[\frac{1}{N} \sum_{i=1,N} (\Delta T_i - \overline{\Delta T})^2 \right]^{1/2}, \tag{9}$$

where ΔT is the weighted average change defined by Eq. (7) and $\overline{\Delta T}$ is the equally weighted average.

3. Results from model-quality assessment

In this section we focus on the order of the model performance based on the two evaluation metrics rather than the general features of the temperature and precipitation climatologies from the AOGCMs, which have been described in a number of previous studies (e.g., Jiang et al. 2005; Zhou and Yu 2006; Xu et al. 2010).

Figure 1 is the plot of model skill scores (M1) of the spatial mean squared error of the temperature (with the scale on the *left*-hand ordinate) and precipitation (with the scale on the *right*-hand ordinate). Models along the *x* axis are ordered by their mean M1 value of both temperature and precipitation. Not surprisingly, in general the spatial skill metric (M1) of temperature is greater than that of precipitation. For the simulation of the temperature pattern, the top three models are the Istituto Nazionale di Geofisica e Vulcanologia ECHAM4 (INGV ECHAM4), ECHAM5–MPI-OM, and the third climate configuration of the Met Office (UKMO) Unified Model (HadCM3C), with the M1 value greater than 0.9. As for the simulation of precipitation, the INGV_ECHAM, the Commonwealth Scientific and Industrial Research Organisation Mark version 3.5 (CSIRO Mk3.5), and the Meteorological Institute of the University of Bonn, ECHO-G Model (MIUBECHOG), whose M1 value is up to 0.6, have relatively higher skill than others. Taking both temperature and precipitation into account, the top three models are INGV_ECHAM4, CSIRO Mk3.5, and UKMO HadCM3, whereas the MMEs rank fourth.

In terms of interannual variability, Fig. 2 depicts the model skill scores (M2 value averaged over China) of the interannual variability (measured by the interannual standard deviation) of both temperature and precipitation. Similar to M1 mentioned above, model skill in simulating the interannual variability of temperature is generally higher than that of precipitation. Overall, the three models that perform best are the INGV ECHAM4, the Meteorological Research Institute Coupled General Circulation Model, version 2.3.2a (MRI CGCM2.3.2), and the HadCM3. In addition, MME has the lowest M2

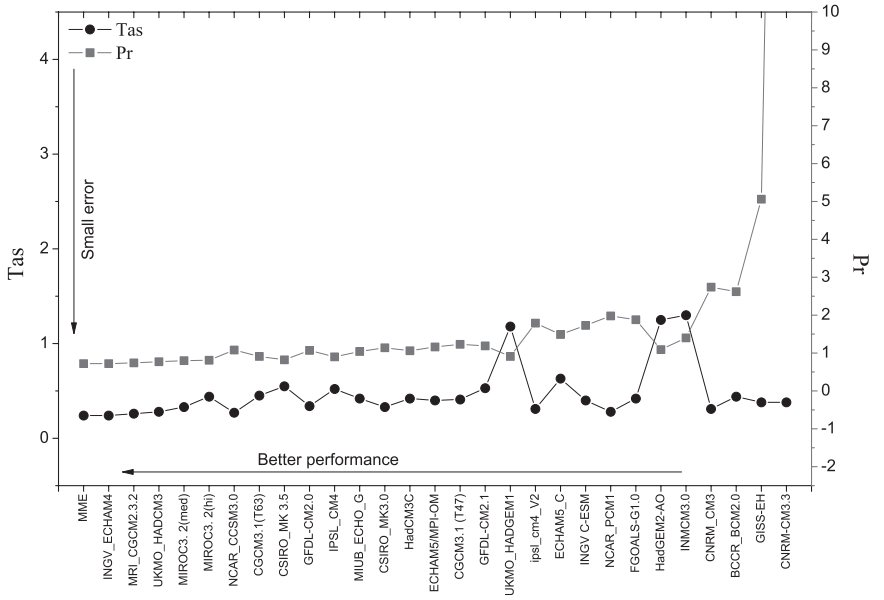

FIG. 2. As in Fig. 1, but for model skill scores (M2) of the interannual variability (measured by the interannual standard deviation) of both temperature and precipitation.

value for both temperature and precipitation, signifying that MME has the best skill in simulating the interannual variability compared to any single model.

By combining information from different performance metrics, the overall ranking and weighting results are shown in Table 2. The weight for each model is calculated based on its ranks according to Eqs. (4) and (5). Note that the weight for each model would be 0.036 in the case that all models were equally weighted. The best five models—namely, the INGV ECHAM4, the UKMO HadCM3, the CSIRO Mk3.5, the National Center for Atmospheric Research (NCAR) Community Climate System Model, version 3 (CCSM3), and the Model for Interdisciplinary Research on Climate 3.2, high-resolution version MIROC3.2(hires)—have weights of 0.289, 0.096, 0.058, 0.048, and 0.044, respectively, clearly better than others. We also notice that 4 of these 5 models (INGV ECHAM4, MIROC3.2(hires), NCAR CCSM3, and CSIRO Mk3.5) have the highest horizontal resolutions (Table 1), indicating that finer model resolutions are needed to simulate present-day climate over China accurately (Gao et al. 2006). The five above-mentioned models are consistently ranked in the top 8 models for both M1 and M2 evaluation criteria. Particularly, INGV ECHAM4 outperforms any other models for both evaluation criteria. Therefore, this model is given the largest weight (0.289). On the other hand, several models [e.g., the Centre National de Recherches Météorologiques Coupled Global Climate Model, version 3.3 (CNRM-CM3.3) and the Goddard Institute for Space Studies Model E-H (GISS-EH)] are given smaller weights (e.g., 0.011) because of their poor performance in the two evaluation metrics.

4. Probabilistic projection of climate change

This section describes future probabilistic changes of the mean values and interannual variability in temperature and precipitation, based on the methodology described in section 2c. We focus on two future time periods under the A1B scenario: one is 2011–40, representing the near-term period, which is of critical importance for policy and decision makers (Meehl et al. 2007; the other is 2070–99, which has the maximal climate change signal. The term *change* refers to the difference between 30-yr means in the scenario and in the reference period (1961–90).

a. Changes in mean temperature and precipitation

Figure 3 shows the probability of winter [December–February (DJF)], summer [June–August (JJA)], and annual mean surface air temperature and precipitation changes (China averaged) exceeding a given threshold as a function of the threshold for 2011–40 and 2070–99. The probability is calculated following Eq. (6), and the W_i for each model is shown in Table 2. According to Eq. (6), as the temperature (or precipitation) change threshold increases, the probability decreases until it reaches 0 above a maximum value, implying that no model projects a greater change than this value.

For the near-term period (2011–40), all models show a positive temperature change over China in all seasons; therefore, the probability of warming is equal to 1. The

TABLE 2. Weights and ranks of the 28 AOGCMs according to their performance. Bold values indicate that the model has a weight >0.036 (value of equally weighted models).

Model ID	Rank of M1	Rank of M2	Sum of the ranks	Weights
INGV ECHAM4	**1**	**1**	**2**	**0.289**
UKMO HadCM3	**3**	**3**	**6**	**0.096**
CSIRO Mk3.5	**2**	**8**	**10**	**0.058**
NCAR CCSM3	**6**	**6**	**12**	**0.048**
MIROC3.2(hires)	**8**	**5**	**13**	**0.044**
MIROC3.2(medres)	12	4	16	0.036
CSIRO Mk3.0	4	12	16	0.036
CGCM3.1 (T63)	11	6	17	0.034
MIUBECHOG	9	11	20	0.029
MRI CGCM2.3.2	20	2	22	0.026
GFDL CM2.1	6	16	22	0.026
GFDL CM2.0	14	9	23	0.025
HadGEM2-AO	4	23	27	0.021
MPI ECHAM5/MPI-OM	14	14	28	0.021
INGV C-ESM	9	20	29	0.020
IPSL CM4	21	9	30	0.019
HadCM3C	19	12	31	0.019
CGCM3.1 (T47)	16	15	31	0.019
ECHAM5_C	13	19	32	0.018
IPSL CM4 V2	17	17	34	0.017
UKMO HadGEM1	18	17	35	0.017
NCAR PCM1	25	21	46	0.013
INM-CM3.0	22	24	46	0.013
IAP FGOALS-g1.0	26	22	48	0.012
BCCR BCM2.0	23	25	48	0.012
CNRM CM3	24	25	49	0.012
CNRM-CM3.3	27	28	55	0.011
GISS-EH	28	27	55	0.011

probability of a temperature change being greater than 1.0°C is also quite high, reaching 0.9 or greater. For a warming level equal to or greater than 1.5°C, the probability decreases sharply to 0.73, 0.24, and 0.21 for DJF, JJA, and the annual mean, respectively. We can see that in winter, the warming has the largest signal. The maximum change is of the order 2.0°–2.5°C. For precipitation, in general there is a positive change in 2011–40 but the amplitude is quite weak. Only in DJF is there a probability greater than 0.5 of an increase in excess of 5%.

For the end of the twenty-first century (2070–99), the general behaviors of the projected changes are similar to that of the period 2011–40 for both temperature and precipitation. However, the magnitudes are much greater. There is a near 100% probability for increases of temperature above 2.5°C for both summer and winter. Furthermore, the probability of exceeding the 3°C threshold reaches 0.9 or greater in all seasons. During winter, this is also true for a warming level above 3.5°C. The maximum change ranges from 5° to 6°C. For precipitation, the probability curves have a similar shape as for temperature, a prevalence of probability of positive change is observed, especially in winter. The probability of the DJF, JJA, and annual mean precipitation change greater than 10% is 0.94, 0.34, and 0.45, respectively. The projected maximum change for precipitation is 60% in winter and 25% in summer.

1) CHANGES IN 2011–40

The probability of exceeding three warming levels (1°, 1.5°, and 2.0°C) over China during winter and summer for 2011–40 under SRES A1B is given in Fig. 4. Shadings indicate areas where the probabilities are greater than 0.5. When the warming level is set to 1.0°C, we obtain probabilities greater than 0.5 for all of China in winter and the northwestern part of China in summer. Similar spatial structures are obtained for a future warming set to >+1.5°C but having a smaller probability of occurring. In addition, over the northeastern part there is a 50% probability of above +2.0°C warming in winter. During summer, most of the high probabilities for above 1°C warming were located over the Tibetan Plateau and the northern parts, encompassing northwest China, north China, and northeast China. The probabilities for a warming level above +2.0°C are quite low, implying that a warming by +2.0°C is unlikely in summer over China.

With respect to the precipitation, Fig. 5 shows the probability for exceeding precipitation change thresholds (0%, 5%, and 10%) during winter (top panel) and summer (bottom panel). Shaded areas indicate probabilities greater than 0.5. In winter the northern parts show probabilities of above 0.5 for rainfall to increase. In the southeastern parts, the probability for rainfall to increase is below 50%, indicating a higher probability for rainfall to decrease in these areas. Increases (5% and 10% levels) are mainly seen in the northern parts (northwest China, north China, and northeast China). During summer the most probable future changes of rainfall are increases in southeast China, east of northeast China, and the Tibetan Plateau, with probabilities higher than 0.5 over those regions.

2) CHANGES IN 2070–99

In general the spatial patterns of probability of exceeding given change thresholds for both temperature and precipitation in 2070–99 under SRES A1B are the same as that of 2011–40, but with larger magnitude.

Figure 6 depicts the spatial pattern of probability for exceeding temperature change thresholds (3°, 4°, and 5°C) for both DJF and JJA. In winter, there is a near 100% probability across most of China for the warming to be above 3°C. For thresholds above 4°C, northeast China, northwest China, and the Tibetan Plateau also exhibit high probabilities, reaching 60% or higher.

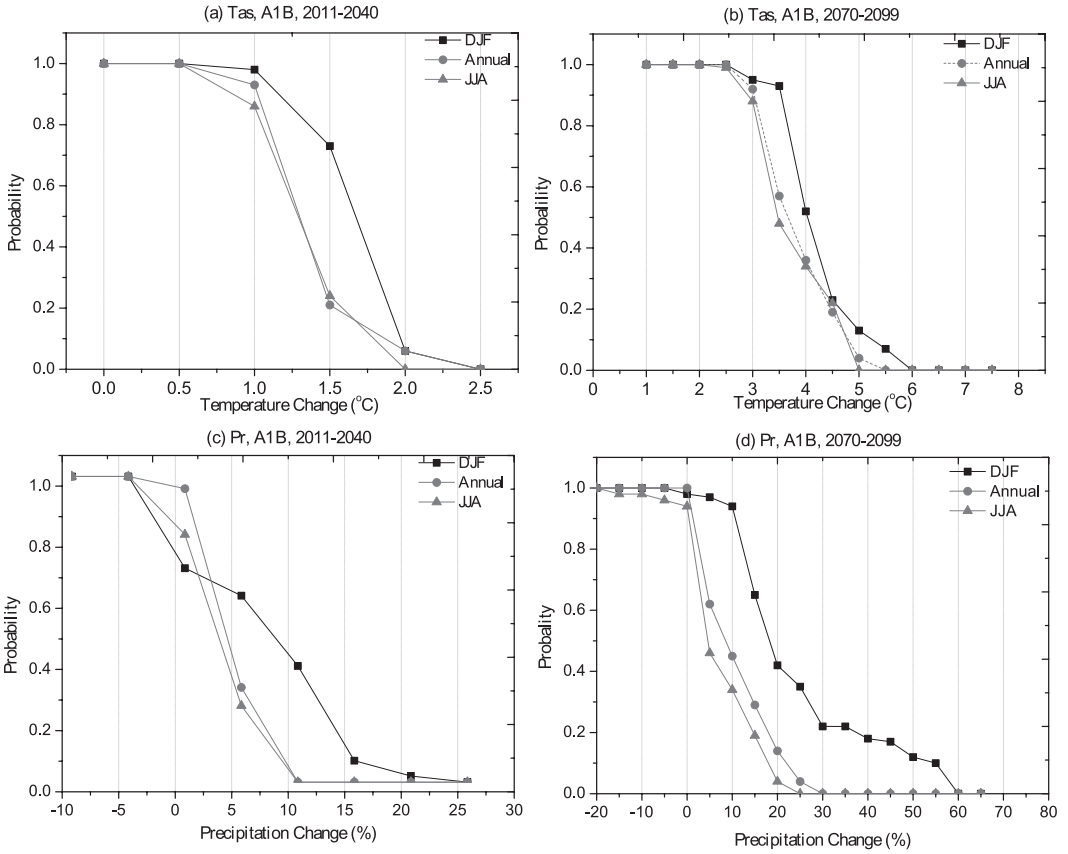

FIG. 3. Probability of surface air temperature and precipitation change (2011–40, 2070–99 minus 1961–90) exceeding given thresholds over mainland China under the A1B scenario: (a) temperature, 2011–2040; (b) temperature, 2070–99; (c) precipitation, DJF; and (d) precipitation, JJA. Units are °C for temperature change and % of present-day value for precipitation change.

Furthermore, over parts of northeast China there is even a 60% probability of above 5°C warming in winter. During summer, most of the high probabilities higher than 50% for future warming above +3°C are located in areas north of 30°N. This is particularly the case for the southern part of northwest China, where the probabilities reach 100%. With respect to the thresholds above 4°C, only the northern part of Xinjiang province exhibits high probabilities. The probability for temperature to increase above 5°C is lower than 20% for most of the regions.

As for changes in precipitation, probabilities for exceeding given thresholds (0%, 10%, and 20%) are shown in Fig. 7. Increases of precipitation mainly appear in the northern parts of China. For instance, there are high probabilities for future increases of winter precipitation by 20% over northeast China, north China, and northwest China. During summer, precipitation increases across the entire country, with the exception of the western part of northwest China. In addition, over southeast China and the eastern part of northwest China, there are high probabilities (greater than 0.5) of increasing by 10%. The probability for rainfall increases above 20% is lower than 0.2 over most of China.

b. Changes in interannual variability

As far as the changes in interannual variability are concerned, we focus on the end of the twenty-first century (2070–99) with the purpose of maximizing the change signal. Figure 8 shows the spatial pattern of probability of exceeding (or not) given change thresholds of temperature interannual variability over China during winter (−0.2°, −0.1°, and 0°C; top) and summer (0°, 0.1°, and 0.2°C; bottom) for the period 2070–99. Areas with a probability greater than 0.5 are shaded. In general, the interannual variability of temperature will increase over most of China in JJA, especially in the northwestern and the central parts, where the probability for increasing above 0.1°C is up to 50% or greater. For temperature in winter, there are areas across China that have probabilities greater than 50% for either increased or decreased interannual variability, consistent with the finding of Xu et al. (2010).

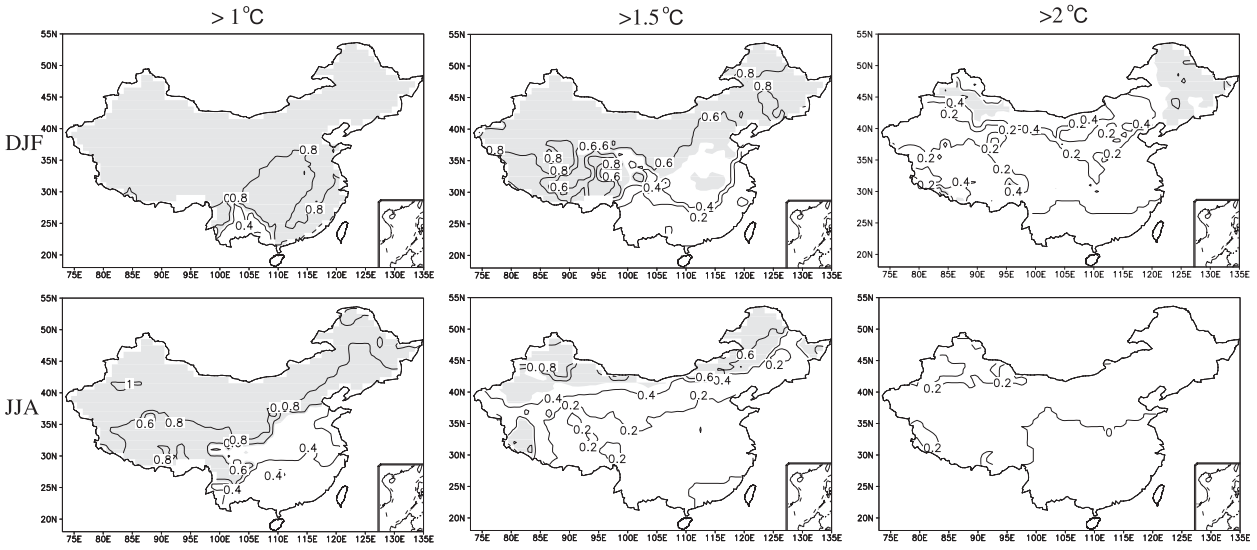

FIG. 4. Spatial pattern of probability for temperature change thresholds of (left) >1°C , (middle) >1.5°C , and (right) >2.0°C over China during (top) winter (DJF) and (bottom) summer (JJA) for the period 2011–40. Shaded areas indicate probabilities >0.5.

For precipitation, there are high probabilities (greater than 60%) across most of China for an enhanced interannual variability of rainfall in both summer and winter (Fig. 9). During winter, most of the high probabilities for future intensification of interannual variability by 20% are located in the northern parts, whereas in summer the southern parts show high probabilities for enhanced interannual variability. In particular, over the Yangtze–Huai River basin (28°–35°N, 105°–120°E), there is a 60% probability of increased ratios of interannual standard deviation of precipitation by 20% in summer, which is much higher than that of the mean precipitation (Fig. 7). It should be noted that previous studies also found that the interannual variability is intensified much more remarkably in comparison with the mean precipitation under global warming conditions (e.g., Lu and Fu 2010), implying that there will be a higher probability of potential floods and droughts in the future over this region.

5. Comparison among a few variants of the methodology

a. Comparison with the equal weighting

The particularity of our methodology resides in the calculation of weights attributed to each model. It is

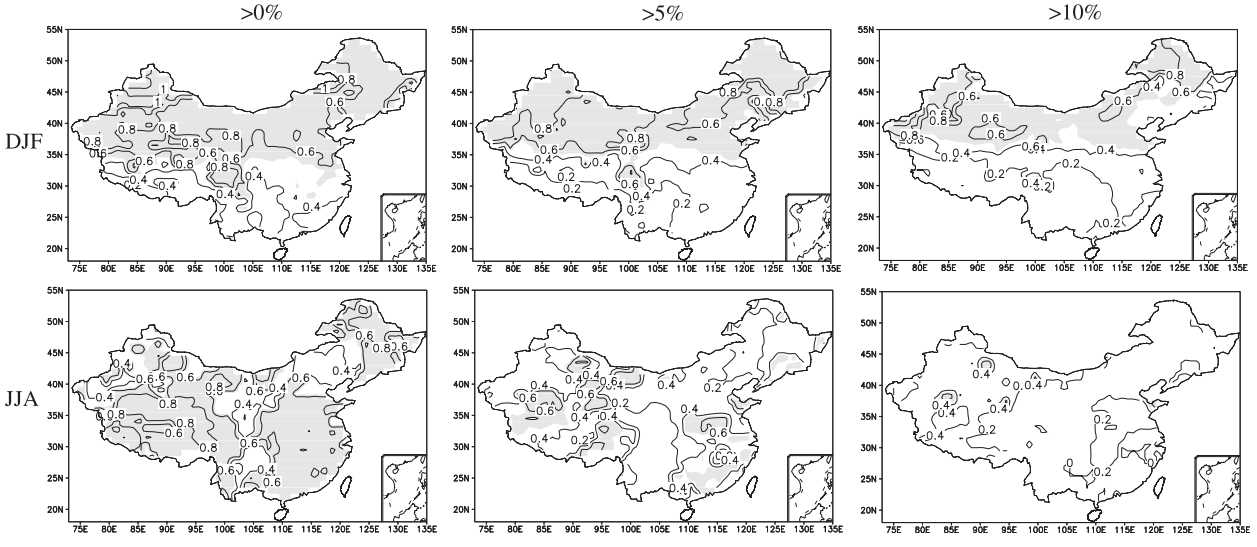

FIG. 5. As in Fig. 4, but for precipitation change thresholds of >0%, >5% and >10%.

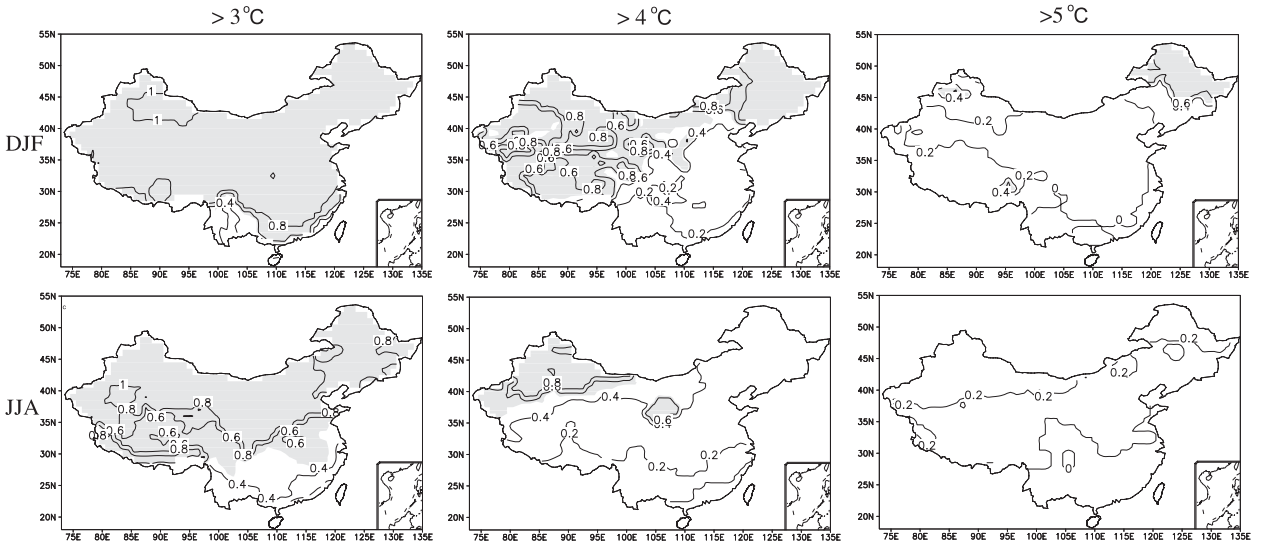

FIG. 6. As in Fig. 4, but for the period 2070–99. Temperature change thresholds are now >3.0°C , >4.0°C, and >5.0°C.

based on a simple and straightforward idea: the relative rank of models in reproducing present-day climate should be used in a proportional way to calculate their weights. How does the weighting affect the projection? We compare now the projected changes of temperature and precipitation over China, calculated by the rank-based weighted average of the 28 AOGCMs [W_mean, basing on Eq. (7)], as well as the simple multimodel average (S_mean, calculated with no weighting, or equal weights). Furthermore, projected changes only from the five best models in Table 2 (Top5_mean) are also shown. The analysis is concentrated for the period of 2070–99.

1) TEMPERATURE

Figure 10 depicts the projected change of surface air temperature over China in both winter and summer for the period of 2070–99 under the A1B scenario, as obtained with the W_mean, S_mean, and Top5_mean approaches. It is evident that for temperature the magnitudes and main spatial patterns of the changes show a quite good consistency among the three approaches. In winter the area-averaged warming over China for W_mean, S_mean, and Top5_mean is 4.27°, 4.28°, and 4.49°C, respectively. Consistent with Xu et al. (2010), the northern parts show greater warming than the

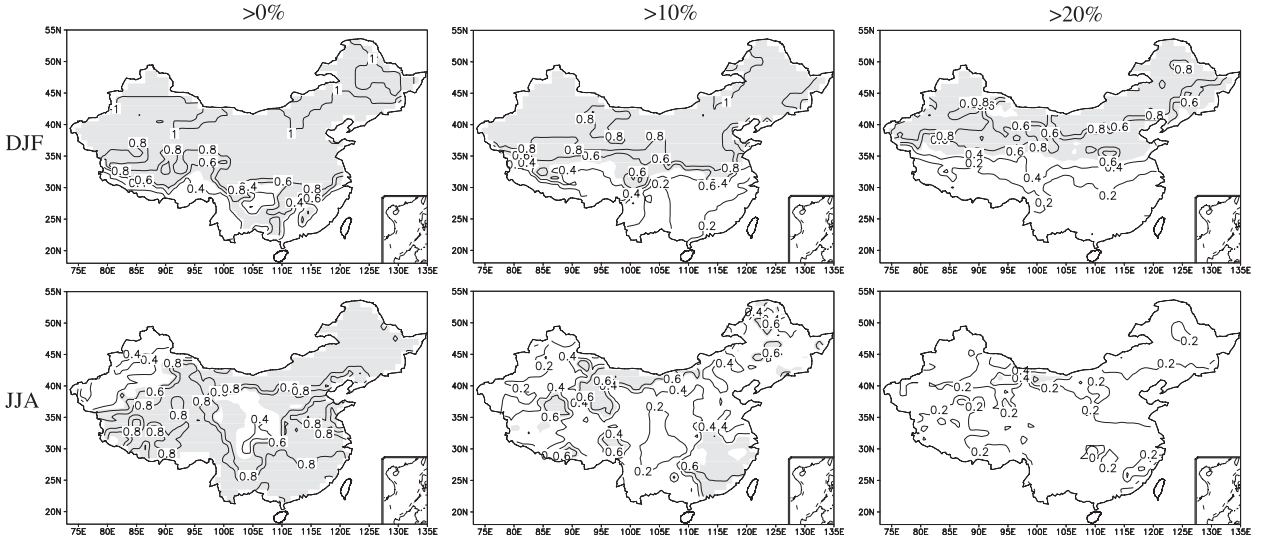

FIG. 7. As in Fig. 5, but for the period 2070–99.

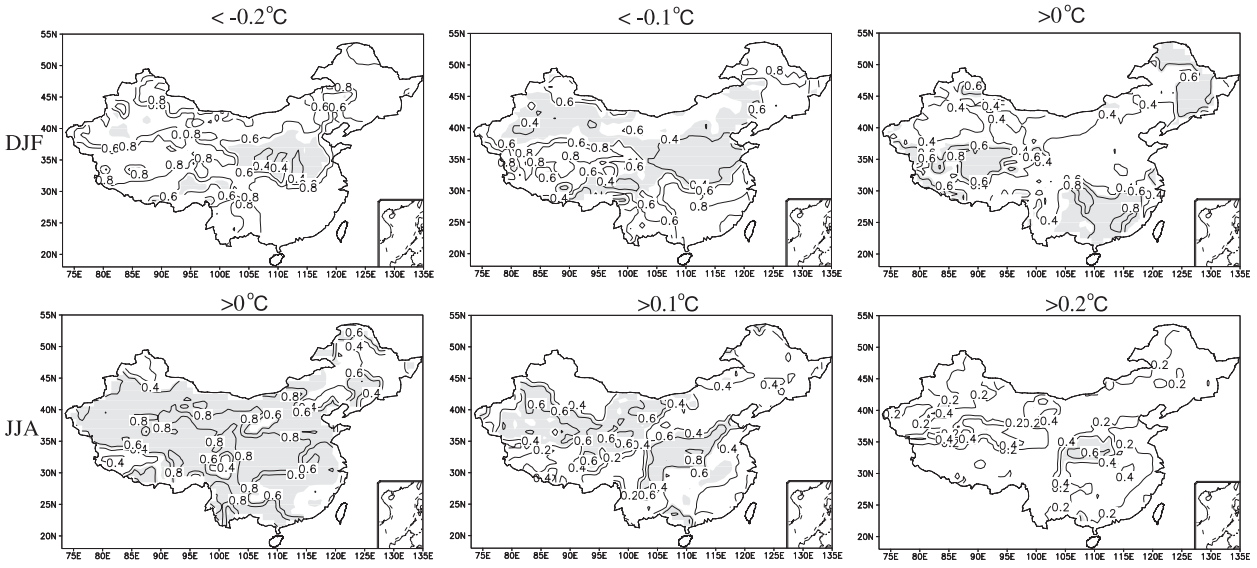

FIG. 8. Spatial patterns over China of cumulative probability for given change thresholds of temperature interannual variability during (top) winter (<−0.2°, <−0.1°, and >0°) and (bottom) summer (>0°, >0.1°, and >0.2°) for the period 2070–99. Shaded areas indicate probabilities >0.5.

southern parts. A large portion of northern China shows warming greater than 4°C, with maximum increases over the northwestern regions (>5°C). In summer the spatial patterns of temperature change are similar to winter, but the magnitudes are slightly smaller than the latter, with the China-averaged warming for W_mean, S_mean, and Top5_mean reaching 3.71°, 3.70°, and 4.00°C, respectively.

2) PRECIPITATION

The changes of DJF and JJA mean precipitation according to W_mean, S_mean, and Top5_mean are given in Fig. 11. Generally speaking, the spatial patterns of this change calculated with the three methods are similar for both seasons. However, there are substantial differences in magnitude, with the largest for Top5_mean, followed by W_mean and S_mean. For instance, the domain-averaged changes in DJF mean precipitation for W_mean, S_mean, and Top5_mean are 24.4%, 21.1%, and 30.3%, respectively. There is a dipolar structure of the precipitation change signal, with an increase over the northern parts of the domain and a decrease in the southern parts. Maximum increases are found in

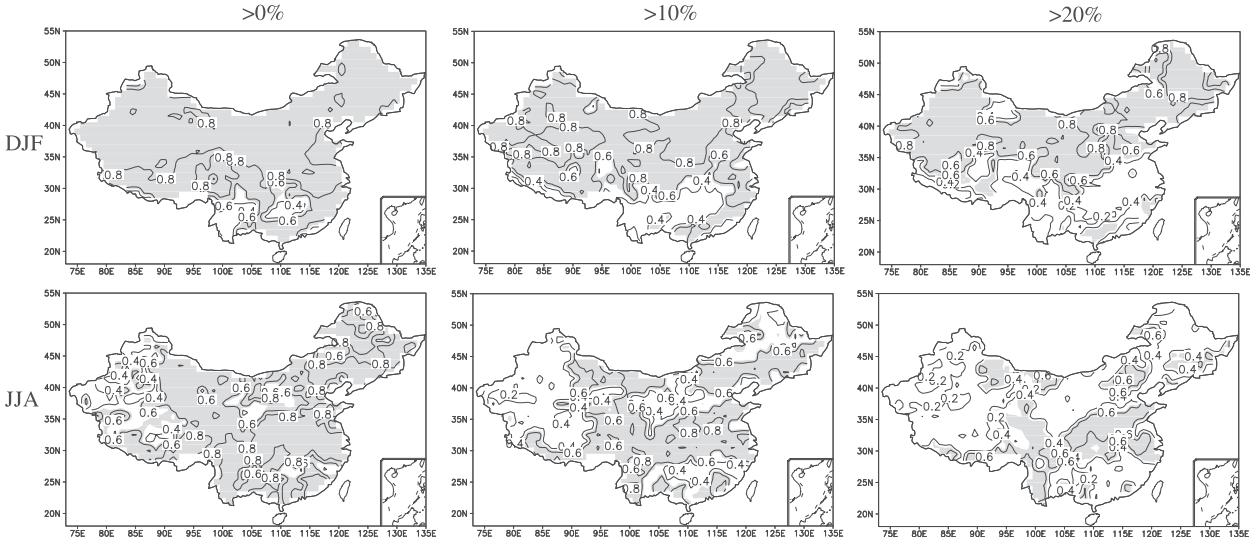

FIG. 9. As in Fig. 8, but for given change thresholds (>0%, >10%, and >20%) of precipitation.

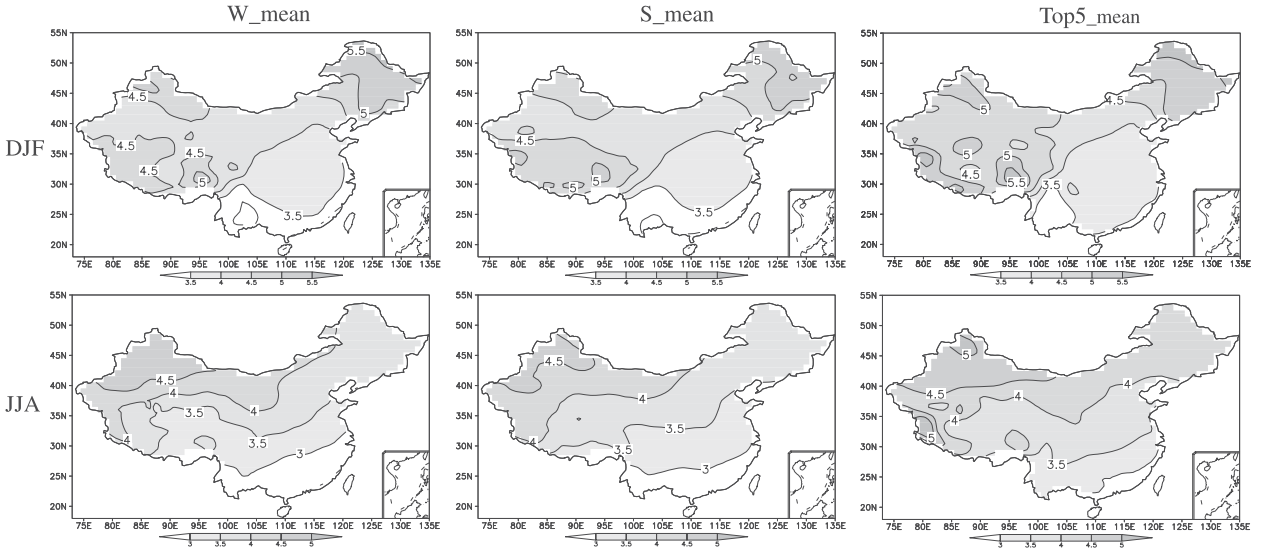

FIG. 10. Temperature changes (2070–99 minus 1961–90, °C) over China in (top) winter (DJF) and (bottom) summer (JJA) under the A1B scenario calculated by (left) W_mean, (middle) nS_mean, and (right) Top5_mean of the top five models [INGV ECHAM4, UKMO HadCM3, CSIRO Mk3.5, NCAR CCSM3, and MIROC3.2(hires)].

northwest China, with the projected changes for W_mean, S_mean, and Top5_mean reaching +50%, +30%, and 70%, respectively. This change pattern is consistent with that of Xu et al. (2010) and may be associated with the intensification of midlatitude cyclones (Christensen et al. 2007) and a poleward shift of the midlatitude storm track in global warming (Yin 2005; Meehl et al. 2007). In summer the projected change of precipitation is positive throughout the entire domain, with an exception in the region around 35°N, 105°E, where weak positive values or even negative values appear. In the western part of northwest China, precipitation is also projected to decrease.

It should be pointed out that when each model is treated equally, probabilistic climate change information from ensembles of AOGCM simulations can also be produced. For example, Raisanen and Palmer (2001) proposed a procedure for estimating probabilities of climate change exceeding given thresholds from ensembles of AOGCM experiments. In their method, this probability is measured by the fraction of the total number of models that simulate a change exceeding the

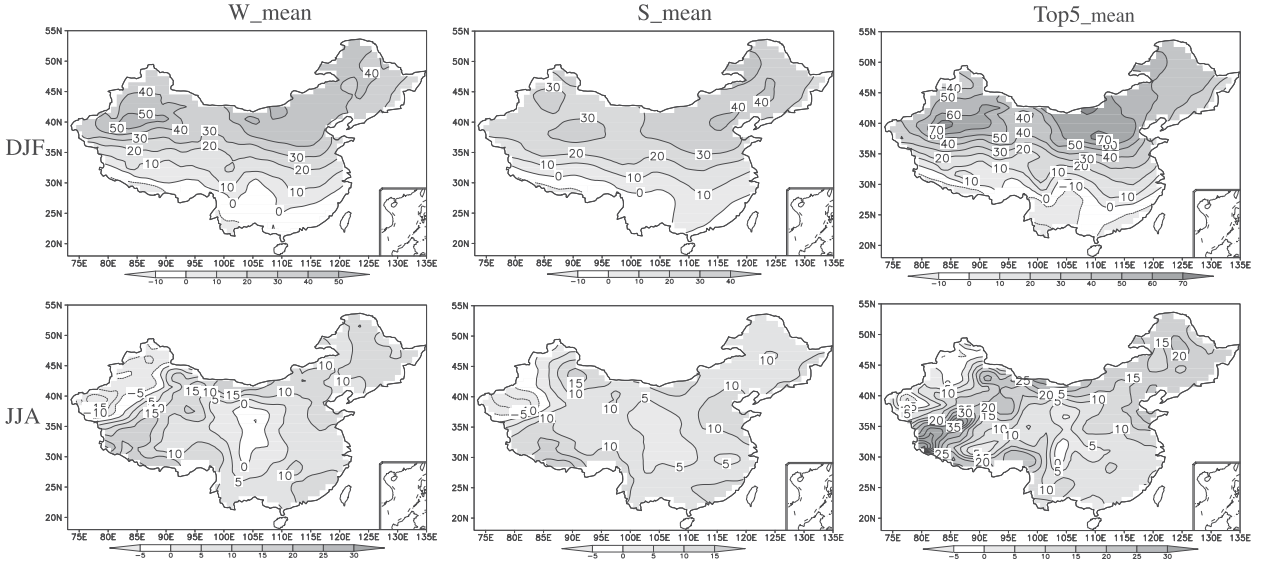

FIG. 11. As in Fig. 10, but for fractional changes of precipitation (%).

TABLE 3. Probability of changes in temperature (ΔT) and precipitation (ΔP) exceeding given thresholds for the rank-based method and the method of Raisanen and Palmer (2001) (in parentheses), for the middle (2020s, 2011–40) and end (2080s, 2070–99) of the twenty-first century.

		DJF					JJA				
2020s	ΔT	≥1°C	≥1.5°C	≥2.0°C	≥2.5°C		≥1°C	≥1.5°C	≥2.0°C		
		0.98 (0.93)	0.73 (0.64)	0.06 (0.07)	0.00 (0.00)		0.86 (0.71)	0.24 (0.21)	0.00 (0.00)		
	ΔP	≥0%	≥5%	≥10%	≥15%	≥20%	≥0%	≥5%	≥10%		
		0.70 (0.93)	0.61 (0.79)	0.38 (0.39)	0.07 (0.11)	0.02 (0.04)	0.81 (0.75)	0.25 (0.21)	0.00 (0.00)		
2080s	ΔT	≥3°C	≥3.5°C	≥4.0°C	≥4.5°C	≥5°C	≥2.5°C	≥3.0°C	≥3.5°C	≥4.0	≥4.5
		0.95 (0.93)	0.93 (0.86)	0.52 (0.64)	0.23 (0.32)	0.13 (0.18)	0.99 (0.96)	0.88 (0.75)	0.48 (0.54)	0.34 (0.39)	0.22 (0.21)
	ΔP	≥0%	≥10%	≥20%	≥30%	≥40%	≥0%	≥5%	≥10%	≥15%	≥20%
		0.98 (0.96)	0.94 (0.89)	0.42 (0.57)	0.22 (0.25)	0.18 (0.18)	0.94 (0.89)	0.46 (0.61)	0.34 (0.36)	0.19 (0.11)	0.04 (0.04)

threshold. Table 3 shows the probability of temperature and precipitation changes being greater than selected thresholds as calculated using our rank-based method and the method of Raisanen and Palmer (2001). In general, the probability trends calculated with the two methods are similar. However, substantial differences are found in some cases, both for temperature and precipitation and for the two periods. For instance, the probability of the increases of DJF mean precipitation by 5% for the period of 2011–40 is 0.61 by the rank-based method, but it reaches 0.79 by the method of Raisanen and Palmer (2001).

An interesting aspect of the aforementioned result is that the weighted model averages are similar to the unweighted ones. Does this mean the weighting is useless? We calculated the RMSD of temperature and precipitation change projected by the weighted mean and the unweighted one at each grid, based on Eqs. (8) and (9), respectively. Table 4 summarizes the China-averaged RMSD of the two methods. Whereas the projected changes of the weighted and unweighted means are similar, the RMSD of the former is smaller than that of the latter, suggesting that there is a decrease in the model spread after weighting. The uncertainties in the projection are reduced to some extent by our method of ranking the models with their performance in present-day climate. This conclusion is consistent with earlier studies (e.g., Schmittner et al. 2005).

b. Comparison with the REA methods

It is interesting to compare our rank-based weighting method with the REA methods (Giorgi and Mearns 2002, 2003; Xu et al. 2010). Xu et al. (2010) introduced the concept of ''effective number of models, or N_{eff}'' ($N_{\text{eff}} = 1/\sum_{i=1}^{N} W_i^2$, where W_i is the weight for each model), which measures the spread of the weights and thus the relative contribution of the different models in the ensemble. The number of models decreases when the weighting is more ''aggressive.'' We calculated the value of N_{eff} of the ranking approach, as well as that of the REA1 (Xu et al. 2010) and REA-ORIG (Giorgi and Mearns 2002; note that in REA-ORIG, the N_{eff} is calculated separately for temperature and precipitation) methods over China, with the annual mean temperature and precipitation of the 28 AOGCMs. The N_{eff} value is 9.0 and 10.5 for the ranking approach and REA1, respectively; and 14.0 and 17.2 for the REA-ORIG (temperature) and REA-ORIG (precipitation) respectively. The N_{eff} value of the ranking approach is smaller than those of the REA methods, implying that generally the former method is more aggressive than the latter.

Coming to the projected change, Fig. 12 depicts the spatial pattern of probability of exceeding given change thresholds (3°, 4°, and 5°C) of annual mean temperature for the period 2070–99, which is calculated by the rank-based weighting method (Rank_W, top panels) and the REA method (REA_Xu, bottom panels) refined by Xu et al. (2010). It is evident that for temperature, the main spatial patterns of the changes show a quite good consistency among the two approaches, but significant differences are found at local scales. For instance, the probability for a warming level above +3.0°C over southern China is lower than 50% as obtained by the rank weighting method; however, the REA result indicates high probabilities for future increases of +3.0°C over this region. For thresholds above 4°C, there are also some differences over northwestern China among the two approaches.

For precipitation, the spatial patterns of this change calculated with the two methods are generally similar (Fig. 13). There are substantial differences at subregions, for example, in the region around 35°N, 105°E, results of

TABLE 4. China-averaged RMSD of ΔT and ΔP calculated by the rank-based weighted averages and the unweighted ones (in parentheses) for end of the twenty-first century (2080s, 2070–99).

ΔT (°C)		ΔP (mm day^{-1})	
DJF	JJA	DJF	JJA
0.87 (0.99)	0.89 (0.95)	0.15 (0.17)	0.47 (0.51)

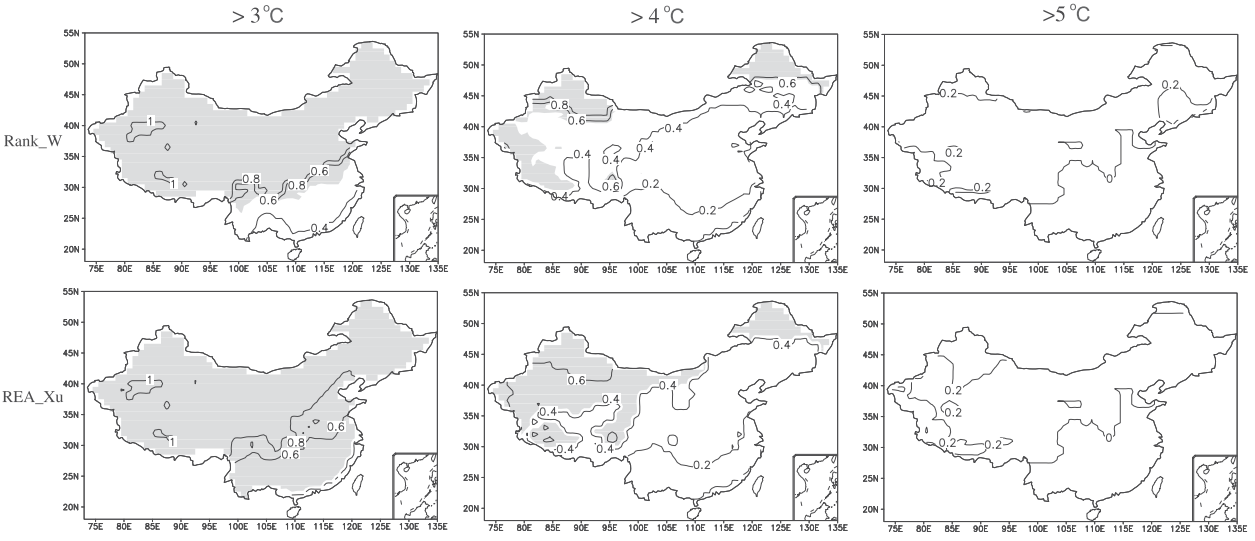

FIG. 12. Spatial pattern of probability for annual mean temperature change thresholds of (left) >3°C, (middle) >4°C, and (right) >5°C over China calculated by (top) Rank_W and (bottom) REA_Xu refined by Xu et al. (2010) for the period 2070–99. Shaded areas indicate probabilities >0.5.

the rank weighting method show high probabilities (up to 0.8) for rainfall to increase; however, in the REA case, the probability for rainfall to increase is below 50%, indicating a higher probability for rainfall to decrease in this area.

6. Summary and conclusions

In the present study, we provided the probabilistic results of climate change over China for the middle and end of the twenty-first century, respective to the control period 1961–90, under the SRES A1B emission scenario. We first ranked the 28 AOGCMs based on their ability to simulate present-day climate over China in terms of two evaluation metrics. Then the models were given with different weights based on their performance for present-day climate. We addressed the issue of uncertainties due to intermodel differences to some extent by approaching the climate projection problem in a probabilistic way. The main finding can be summarized as follows:

1) By combining evaluation information from different performance metrics and different variables, the overall ranking and weighting results show that five models that have relatively higher resolutions—namely, INGV ECHAM4, UKMO HadCM3, CSIRO Mk3.5, NCAR CCSM3.0, and MIROC3.2(hires)

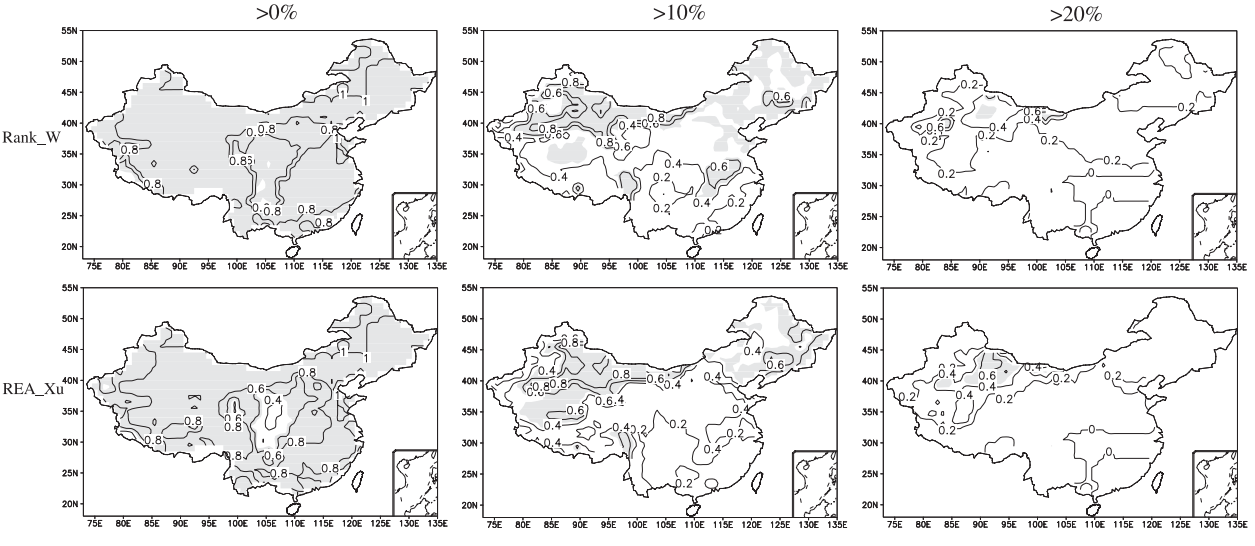

FIG. 13. As in Fig. 12, but for annual mean precipitation change thresholds of (left) >0%, (middle) >10%, and (right) >20%.

clearly perform better than others over China. Their corresponding weights are 0.289, 0.096, 0.058, 0.048, and 0.044, respectively.

2) Surface air temperature is projected to increase significantly for both the middle and end of the twenty-first century under A1B scenario, with larger magnitude over the north in winter. For instance, in winter for the period 2070–99 there is a near 100% probability across most of China for temperature to increase above 3°C. For thresholds above 4°C, northeast China, northwest China, and the Tibetan Plateau exhibit high probabilities, reaching 60% or higher. During summer, most of the high probabilities (greater than 50%) for a future warming above +3°C are located in areas north of 30°N.
3) There are significant increases in rainfall in the twenty-first century under the A1B scenario, especially for the period 2070–99. For example, there are high probabilities (greater than 50%) for future increases of winter precipitation by 20% over northeast China, north China, and northwest China. During summer, high probabilities of precipitation increasing by 10% mainly appear in southeast China and in the eastern part of northwest China.
4) In general, the interannual variability of temperature will increase over most of China in JJA, especially in the northwestern and the central parts; whereas in winter, there are areas across China that have probabilities of greater than 50% for either increased or decreased interannual variability. For precipitation, during winter, most of the high probabilities for future intensification of interannual variability by 20% are located in the northern parts, whereas in summer the southern parts show high probabilities for enhanced interannual variability. In particular, over the Yangtze–Huai River basin (28°–35°N, 105°–120°E), there is a 60% probability of increased interannual standard deviation of precipitation by 20% in summer, which is much higher than that of the mean precipitation.
5) There are small differences between the weighted and unweighted projections, but a decrease in the model spread is found in the former. Compared with the REA methods, the rank-based weighting method is more aggressive.

Probabilistic projection of climate changes at both global and regional scales is still in the early stage of development, and there is a lack of consensus on how models should be best evaluated and weighted; in other words, the best way of performing the weighting is hard to determine, and there is no method that has yet won widespread acceptance (Raisanen et al. 2010; Weigel et al. 2010). In the present study, we only focus on two evaluation metrics based on the monthly-mean surface air temperature and precipitation. The method of producing weights is relatively simple and based on the rank attributed to each model. Moreover, there is always an element of subjectivity to some extent. It is clear that more research will be needed to produce probabilistic results of climate change based on new statistical methods (e.g., in a Bayesian framework and machine learning) and more comprehensive evaluation metrics, such as processes evaluation (more relevant for issues on climate change) and climate extremes (e.g., Chen et al. 2011; Jiang et al. 2011), rather than focusing only on temperature and precipitation (Knutti et al. 2010; Knutti 2010).

Acknowledgments. We thank all the modeling groups, the PCMDI, and the WCRP's WGCM for their roles in producing or making available the WCRP CMIP3 multimodel dataset. Support of this dataset is provided by the Office of Science, U.S. Department of Energy. The ENSEMBLES data used in this work were funded by the EU FP6 integrated project ENSEMBLES. This work is supported by the Chinese National Science Foundation (Grant 40875058), the National Key Technologies R&D Program under Grant 2007BAC29B03, the Natural Science Foundation of Jiangsu Province under Grant 07KJA17020, and the Research and Innovation Project for College Graduates of Jiangsu Province (Grant CX09B_229Z), as well as a Project Funded by the Priority Academic Program Development (PAPD) of Jiangsu Higher Education Institutions. We also thank three anonymous reviewers for their very constructive comments and suggestions that greatly improved this manuscript.

REFERENCES

Chen, W., Z. Jiang, L. Li, and P. Yiou, 2011: Simulation of regional climate change under the IPCC A2 scenario in southeast China. *Climate Dyn.,* **36,** 491–507, doi:10.1007/s00382-010-0910-3.

Christensen, J. H., and Coauthors, 2007: Regional climate projections. *Climate Change 2007: The Physical Science Basis,* S. Solomon et al., Eds., Cambridge University Press, 847–940.

Collins, M., 2007: Ensembles and probabilities: A new era in the prediction of climate change. *Philos. Trans. Roy. Soc. London,* **A365,** 1957–1970.

Cubasch, U., and Coauthors, 2001: Projections of future climate change. *Climate Change 2001: The Scientific Basis,* J. T. Houghton et al., Eds., Cambridge University Press, 525–582.

Furrer, R., R. Knutti, S. R. Sain, D. W. Nychka, and G. A. Meehl, 2007: Spatial patterns of probabilistic temperature change projections from a multivariate Bayesian analysis. *Geophys. Res. Lett.,* **34,** L06711, doi:10.1029/2006GL027754.

Gao, X., Y. Xu, Z. C. Zhao, J. S. Pal, and F. Giorgi, 2006: On the role of resolution and topography in the simulation of East Asia precipitation. *Theor. Appl. Climatol.,* **86,** 173–185.

Giorgi, F., and L. O. Mearns, 2002: Calculation of average, uncertainty range, and reliability of regional climate changes from AOGCM simulations via the ''reliability ensemble averaging'' (REA) method. *J. Climate,* **15,** 1141–1158.

——, and ——, 2003: Probability of regional climate change based on the reliability ensemble averaging (REA) method. *Geophys. Res. Lett.,* **30,** 1629, doi:10.1029/2003GL017130.

Gleckler, P. J., K. E. Taylor, and C. Doutriaux, 2008: Performance metrics for climate models. *J. Geophys. Res.,* **113,** D06104, doi:10.1029/2007JD008972.

Greene, A. M., L. Goddard, and U. Lall, 2006: Probabilistic multimodel regional temperature change projections. *J. Climate,* **19,** 4326–4346.

Jiang, D., H. Wang, and X. Lang, 2004: Multimodel ensemble prediction for climate change trend of China under SRES A2 scenario (in Chinese). *Chin. J. Geophys.,* **47,** 776–784.

——, ——, and ——, 2005: Evaluation of East Asian climatology as simulated by seven coupled models. *Adv. Atmos. Sci.,* **22,** 479–495.

——, Y. Zhang, and J. Sun, 2009: Ensemble projection of 1-3°C warming in China. *Chin. Sci. Bull.,* **54,** 3326–3334.

Jiang, Z., J. Song, L. Li, W. Chen, Z. Wang, and J. Wang, 2011: Extreme climate events in China: IPCC-AR4 model evaluation and projection. *Climatic Change,* doi:10.1007/s10584-011-0090-0, in press.

Knutti, R., 2010: The end of model democracy? An editorial comment. *Climatic Change,* **102,** 395–404.

——, R. Furrer, C. Tebaldi, J. Cermak, and G. A. Meehl, 2010: Challenges in combining projections from multiple climate models. *J. Climate,* **23,** 2739–2758.

Li, H., L. Feng, and T. Zhou, 2010: Multi-model projection of July–August climate extreme changes over China under CO_2 doubling. Part I: Precipitation. *Adv. Atmos. Sci.,* **28,** 433–447, doi:10.1007/s00376-010-0013-4.

Lu, R., and Y. Fu, 2010: Intensification of East Asian summer rainfall interannual variability in the twenty-first century simulated by 12 CMIP3 coupled models. *J. Climate,* **23,** 3316–3331.

Meehl, G. A., and Coauthors, 2007: Global climate projections. *Climate Change 2007: The Physical Science Basis,* S. Solomon et al., Eds., Cambridge University Press, 747–846.

Mitchell, T. D., and P. D. Jones, 2005: An improved method of constructing a database of monthly climate observations and associated high-resolution grids. *Int. J. Climatol.,* **25,** 693–712, doi:10.1002/joc.1181.

Moise, A. F., and D. A. Hudson, 2008: Probabilistic predictions of climate change for Australia and southern Africa using the reliability ensemble average of IPCC CMIP3 model simulations. *J. Geophys. Res.,* **113,** D15113, doi:10.1029/2007JD009250.

Nakicenovic, N., and R. Swart, Eds., 2000: *Special Report on Emissions Scenarios.* Cambridge University Press, 599 pp.

New, M., D. Lister, M. Hulme, and I. Makin, 2002: A high-resolution data set of surface climate over global land areas. *Climate Res.,* **21,** 1–25, doi:10.3354/cr021001.

Perkins, S. E., and A. J. Pitman, 2009: Do weak AR4 models bias projections of future climate changes over Australia? *Climatic Change,* **93,** 527–558.

Pierce, D. W., T. P. Barnett, B. D. Santer, and P. J. Gleckler, 2009: Selecting global climate models for regional climate change studies. *Proc. Natl. Acad. Sci. USA,* **106,** 8441–8446.

Raisanen, J., and T. N. Palmer, 2001: A probability and decision-model analysis of a multimodel ensemble of climate change simulations. *J. Climate,* **14,** 3212–3226.

——, L. Ruokolainen, and J. Ylhaisi, 2010: Weighting of model results for improving best estimates of climate change. *Climate Dyn.,* **35,** 407–422.

Santer, B. D., and Coauthors, 2009: Incorporating model quality information in climate change detection and attribution studies. *Proc. Natl. Acad. Sci. USA,* **106,** 14 778–14 783.

Scherrer, S. C., 2010: Present-day interannual variability of surface climate in CMIP3 models and its relation to future warming. *Int. J. Climatol.,* **31,** 1518–1529, doi:10.1002/joc.2170.

Schmittner, A., M. Latif, and B. Schneider, 2005: Model projections of the North Atlantic thermohaline circulation for the 21st century assessed by observations. *Geophys. Res. Lett.,* **32,** L23710, doi:10.1029/2005GL024368.

Smith, R. L., C. Tebaldi, D. Nychka, and L. O. Mearns, 2009: Bayesian modeling of uncertainty in ensembles of climate models. *J. Amer. Stat. Assoc.,* **104,** 97–116.

Sun, Y., and Y. Ding, 2008: Validation of IPCC AR4 climate models in simulating interdecadal change of East Asian summer monsoon (in Chinese). *Acta Meteor. Sin.,* **66,** 765–780.

——, and ——, 2009: A projection of future changes in summer precipitation and monsoon in East Asia. *Sci. China,* **D53,** 284–300, doi:10.1007/s11430-009-0123-y.

Taylor, K. E., R. J. Stouffer, and G. A. Meehl, 2008: A summary of the CMIP5 experiment design. [Available online at http://cmip-pcmdi.llnl.gov/cmip5/docs/Taylor_CMIP5_dec31.pdf.]

Tebaldi, C., and R. Knutti, 2007: The use of the multi-model ensemble in probabilistic climate projections. *Philos. Trans. Roy. Soc. London,* **A365,** 2053–2075.

——, and B. Sanso, 2009: Joint projections of temperature and precipitation change from multiple climate models: A hierarchical Bayesian approach. *J. Roy. Stat. Soc.,* **A172,** 83–106.

——, L. O. Mearns, D. Nychka, and R. L. Smith, 2004: Regional probabilities of precipitation change: A Bayesian analysis of multimodel simulations. *Geophys. Res. Lett.,* **31,** L24213, doi:10.1029/2004GL021276.

——, R. W. Smith, D. Nychka, and L. O. Mearns, 2005: Quantifying uncertainty in projections of regional climate change: A Bayesian approach to the analysis of multi-model ensembles. *J. Climate,* **18,** 1524–1540.

van der Linden, P., and J. F. B. Mitchell, Eds., 2009: ENSEMBLES: Climate change and its impacts at seasonal, decadal and centennial timescales. Met Office Hadley Centre, 160 pp.

Watterson, I. G., 2008: Calculation of probability density functions for temperature and precipitation change under global warming. *J. Geophys. Res.,* **113,** D12106, doi:10.1029/2007JD009254.

Weigel, A. P., R. Knutti, M. A. Liniger, and C. Appenzeller, 2010: Risks of model weighting in multimodel climate projections. *J. Climate,* **23,** 4175–4191.

Whetton, P., I. Macadam, J. Bathols, and J. O'Grady, 2007: Assessment of the use of current climate patterns to evaluate regional enhanced greenhouse response patterns of climate models. *Geophys Res. Lett.,* **34,** L14701, doi:10.1029/2007GL030025.

Xu, Y., X. Gao, and F. Giorgi, 2010: Upgrades to the reliability ensemble averaging method for producing probabilistic climate-change projections. *Climate Res.,* **41,** 61–81, doi:10.3354/cr00835.

Yin, J. H., 2005: A consistent poleward shift of the storm tracks in simulations of 21st century climate. *Geophys. Res. Lett.,* **32,** L18701, doi:10.1029/2005GL023684.

Zhou, T., and R. Yu, 2006: Twentieth-century surface air temperature over China and the globe simulated by coupled climate models. *J. Climate,* **19,** 5843–5858.